Advances in Concrete Construction, *Vol. 5, No. 6 (2017) 625-638*
DOI: https://doi.org/10.12989/acc.2017.5.6.625

Study on behavior of RCC beams with externally bonded FRP members in flexure

Sumathi A.* and Arun Vignesh S.

School of Civil Engineering, SASTRA University, Thanjavur 613401, India

(Received May 1, 2017, Revised September 26, 2017, Accepted December 6, 2017)

Abstract. The flexural behavior of Fiber reinforced polymer (FRP) sheets has gained much research interest in the flexural strengthening of reinforced concrete beams. The study on flexure includes various parameters like increase in strength of the member due to the externally bonded (EB) Fiber reinforced polymer, crack patterns, debonding of the fiber from the structure, scaling, convenience of using the fibers, cost effectiveness, etc. The present work aims to study experimentally about the reasons behind the failure due to flexure of an externally bonded FRP concrete beam. In the design of FRP-reinforced concrete structures, deflection control is as critical as much as flexural strength. A numerical model is created using Finite element (FEM) software and the results are compared with that of the experiment.

Keywords: GFRP; CFRP; flexural study; external bonding; numerical analysis

1. Introduction

Fibre reinforced composites have been widely used to strengthen reinforced concrete (RC) members. Mostly because they have a high strength-to-weight ratio, require relatively limited time to cure, and have mechanical properties that can be engineered to meet the desired structural performance. A fibre-reinforced polymer (FRP) composite is made up of continuous fibres and a thermosetting organic resin. It is currently the most common type of composite system used for structural strengthening applications. Fibre reinforced cementitious matrices (FRCM) composite was another type of composite that was recently developed which contains continuous fibres with a cementitious (inorganic) matrices. The substantial increase in energy absorption capacity is the most significant improvement imparted by adding fibres to a concrete. The FRP laminates were produced by the process called pultrusion. Pultrusion technology of manufacturing of fiber composites with polymer matrices appears to be energy-efficient and resource-saving. Pultruded FRP sections are usually made by pultrusion process. This process creates continuous composite profile by pulling raw composites through a heated die. Pultrusion combines words “pull” and “extrusion” where extrusion is pulling of material such as fiberglass and resin, through a shaping die. The reinforcement materials like fibers or woven or braided strands are impregnated with resin, possibly followed by a separate performing system, and pulled through a heated stationary

*Corresponding author, Assistant Professor, E-mail: sumathi@civil.sastra.edu

Copyright © 2017 Techno-Press, Ltd.
http://www.techno-press.org/?journal=acc&subpage=7 ISSN: 2287-5301 (Print), 2287-531X (Online)

die where the resin undergoes polymerization. The impregnation is either done by pulling the reinforcement of a bath or by injecting the resin into an injection chamber which typically is connected to the die. At the end of the pultrusion machine there is a cut-off saw. Pultruded profiles are cut to the specific length and stacked for delivery. The strengthening effect of EB-FRP using composite elements involving glass fibre was studied (Al-Tamimi *et al.* 2014) Use of glass fibre laminates in composite sections with external bonding is well established. Flexural response was better recorded using the epoxy adhesive. Use of carbon – glass hybrid was studied the stiffness contribution of the composite in bridge decks in rehabilitation (Chakrabortty *et al.* 2014). The results of the uniaxial compression tests performed under displacement control condition, a stress-strain relationship of fiber concrete in compression was derived (Hong *et al.* 2011). The numerical model was developed and the results are validated with the experimental bending tests of FRP in slabs (Balsamo *et al.* 2013). Parameters varied here were thickness and the effect of changing the thickness is studied under the four-point loading test (Barros *et al.* 2013). An increase in the width of the FRP will produce an increase in the load-carrying capacity. Interfacial crack propagation and strain distribution of shear debonding are influenced by the width of the FRP laminate in comparison to that of the beam (Sneed *et al.* 2016). Variation in mechanical properties in terms of composite carbon, composite glass sheets and their hybrid combinations is by their hybrid combinations. Different failure modes that can occur were also studied (Subramaniam *et al.* 2007). Studies show that strength increases provided by SRP bonded with cementitious grout were smaller than those obtained using epoxies (Hawileh *et al.* 2015a). Although use of cementitious matrices is in practice, the transfer of stresses was found to be more efficient with epoxy strengthening adhesive (Porta *et al.* 2014). Experimental and analytical investigation of the behavior of Reinforced Concrete (RC) beams strengthened in flexure by means of different combinations of externally bonded hybrid Glass and Carbon Fiber Reinforced Polymer (GFRP/CFRP) sheets were studied based on mechanical properties and concluded that increase in the load capacity of the strengthened beams ranged from 30% to 98% of the unstrengthened control RC beam depending on the combination of the Carbon/Glass sheets and also enhanced the ductility both experimentally and numerically (Rami *et al*. 2014b). Failure modes of reinforced concrete beams strengthened in flexure with externally bonded FRP sheets was analyzed and found that width of FRP sheet plays a role in the failure modes also reported that wider sheets with equal cross sections will give better strengthening results by reducing the bond stress between the concrete surface and the FRP sheets leading to higher flexural beam strength (Thomsen *et al.* 2004). Numerical investigation of plate debonding and performance of reinforced concrete (RC) beams externally strengthened with bonded Carbon Fiber Reinforced Polymers (CFRP) plates running for a length covering 25% of the shear span. The results are compared with plates covering 85% of the shear span in addition to a control unstrengthened specimen and concluded that the developed FE models are capable of accurately predicting and capturing capacity the debonding failure mode of RC beams strengthened with FRP plates (Rami *et al*. 2013c). Experimentally studied the effectiveness of strengthening concrete beams using FRP plates. Numerical model was developed using ANSYS to validate the experimental results reported (Al-Rousan *et al.* 2013). The results showed a significant increase in stiffness and ultimate strength for beams strengthened with FRP plates and investigated the strength and ductility of reinforced concrete beams repaired with CFRP laminates. They examine the effects of retrofitting on strength, deflection, curvature and energy. From the results concluded that suitably designed and positioned external anchorages enabled more ductile failures of the CFRP strengthened beams (Hamid Rahimi *et al*. 2001). Non-linear finite element model was created and validated the

Table 1 Beam details

B1	Normal RCC beam as control specimen
B2	Beam externally bonded with GFRP plate of 2 mm thickness
B3	Beam externally bonded with CFRP plate of 2 mm thickness
B4	Beam externally bonded with CFRP (1 mm) and GFRP (2 mm)
B5	Beam externally bonded with CFRP (2 mm) and GFRP (1 mm)

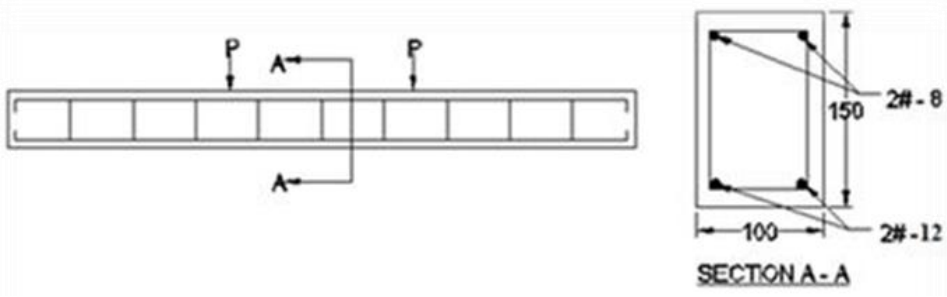

Fig. 1 Beam reinforcement details

experimental results of the behavior of strengthened sulfate damaged reinforced concrete beams. They concluded that glass strips provided at an angle of 45 degrees to the horizontal are effective in strengthening the beams in the shear region. The objective of this paper is to investigate the flexural behavior of control beams and EB-FRP beams to study effectively the load-deflection behavior, energy absorption capacity and crack patterns. Numerical model was developed using ANSYS to validate the experimental results.

2. Experimental program

2.1 Materials and mix proportions

Cement used in the study is Ordinary Portland Cement of grade 43 with specific gravity 3.1, (IS 2269 1997). Sand conforms to zone II (IS 383 1970) with fineness modulus and specific gravity as 3.24 and 2.63 respectively (IS 2386 1986). Corresponding values for coarse aggregate of 20 mm were 6.78 and 2.65. Concrete of M50 mix with proportion 1:0.8:2.13(Cement: FA: CA). The addition of high range water reducer reduced the w/c ratio to 0.32 and the workability was verified with slump cone test.

2.2 Specimens for study

Cubes (150 mm×150 mm) were cast to check the characteristics compressive strength of the concrete mix. Five groups of beams (B1, B2, B3, B4 and B5) were cast. Three in each group of beams had a span of 1200 mm and rectangular cross section of 150×100 mm. Beams were reinforced with two numbers of 12 mm diameter bars as tension reinforcements, along with two numbers of 8 mm diameter bars as hanger bars in compression zone. These bars were tied with 6

Fig. 2 FRP laminates on the tension side of the beam

Table 2 Properties of loctite

Technology	Acrylic
Chemical type	Dimethacrylate ester
Appearance (uncured)	Blue liquid
Viscosity	Medium
Components	One component-requires no mixing
Fluorescence	Positive under UV light
Strength	Medium
Surface cleaner	Loctite 7061

Table 3 Properties of FRP laminates

Property	Unit	CFRP	GFRP
Density	g/cm^3	1.5	1.8
Width	mm	100	100
Thickness	mm	2,1	2,1
Length	mm	1000	1000
Ultimate Tensile Strength	MPa	550	530
Poisson's ratio	-	0.28	0.28
Yield stress (σ_y)	MPa	200	125
Elastic modulus	GPa	1.5	26

Source: Veermak Fibres, Coimbatore, Tamil nadu, India

mm a stirrups bar at 150 mm spacing is shown in Fig. 1. The most widely applied basic FRP strengthening technique, involves the manual application of hand lay-up or prefabricated systems by means of uncured adhesive bonding. A beam with FRP on the tension zone of the beam is shown in Fig. 2. Beam details and properties of adhesives as per Manufacturer manual are shown in Tables 1 and 2 respectively. Properties of GFRP and CFRP laminates are shown in Table 3.

Fig. 3 Test set up for flexure test

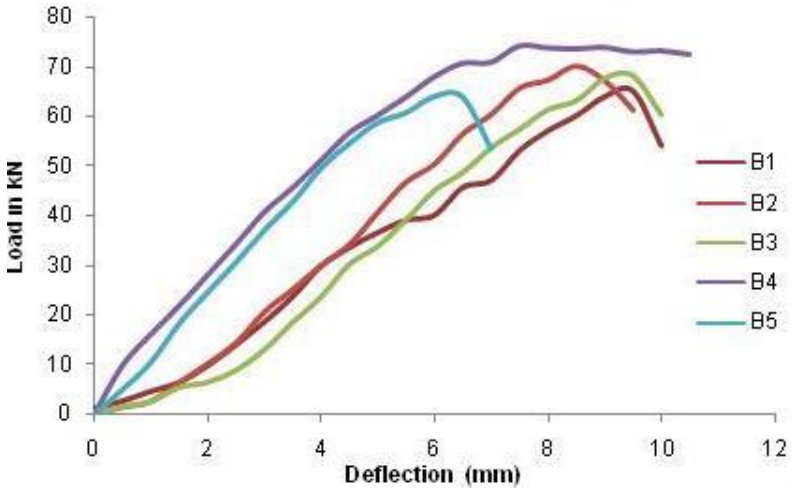

Fig. 4 Load-deflection plot

2.3 Flexure test on beams

To study the strength and stiffness of specimens, two point flexure tests were carried out using self balancing frame as shown in Fig. 3. The test setup includes two point loading using a single point loading system by which the loads are transferred equally to the two points using a spreader beam and two rollers. Deflections were measured in the beam by placing strain gauges at the bottom of the beam. Strains occurring at the points were also measured under using a LVDT strain gauge that was placed at particular intervals. The gauge length between the force points is 333.33 mm in the top and 100 mm from either corner of the beam at the supports. All the specimens were capped for uniform loading prior testing. The control of load over the test was 10 kN/min. All the data like displacement, load and strain were recorded using Automatic data acquisition system which in turn connected to the computer.

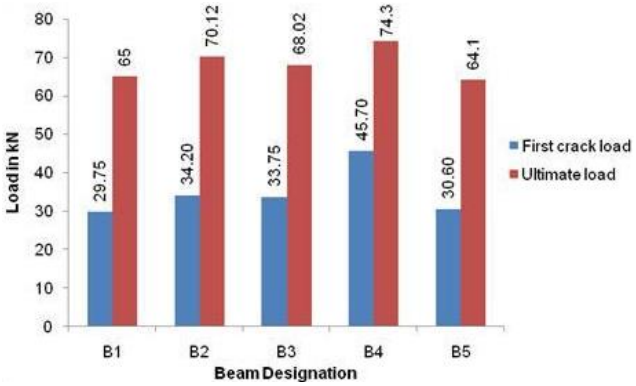

Fig. 5 Ultimate and first crack load for different beams

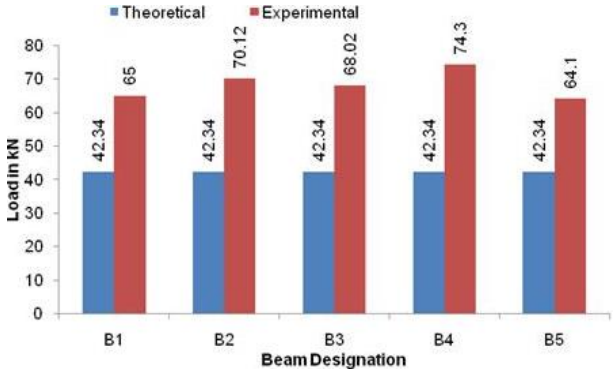

Fig. 6 Load carrying capacity of beams

3. Results and discussion

3.1 Load deflection behavior

Load-deflection curve of tested beams was shown in Fig. 4. An overall evaluation of the load-deflection curves indicates that beams with B4 and B2 laminates exhibit higher load carrying capacity and ductility than control beam. Fig. 5 gives the load results at first crack, ultimate load of control and EB-FRP beams. The first crack loads were obtained through visual examination (B4) exhibit a maximum increase of 53.61% compared with the control specimen B1. The ultimate loads were obtained at the loading stage beyond which the beam would not sustain additional deformation at the same load intensity was exhibited by the above said mix with a maximum increase of 13.85%.

3.2 Load carrying capacity of beams

The loads carried by the control and EB-FRP beams during testing are shown in Fig. 6. The load taken by the beams with EB-FRP increases thereby increase in the flexural strength. The maximum theoretical ultimate load for the beams was found to be 42.34 kN and maximum experimental ultimate load for the beam (B4) was 74.3 kN. There was a 75.48% increase in the

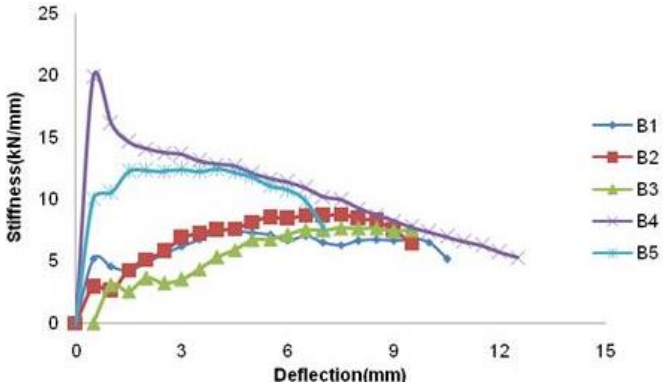

Fig. 7 Stiffness curve for beams

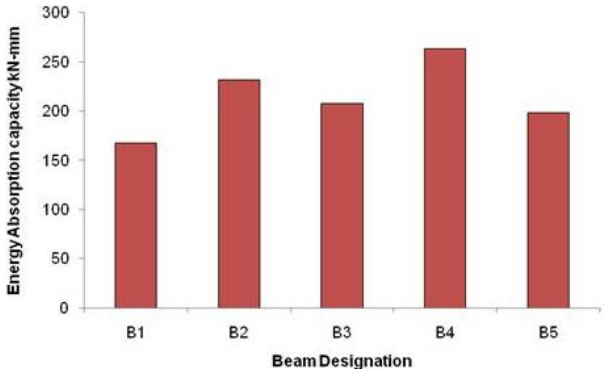

Fig. 8 Energy absorption capacity of the beams

load carrying capacity in EB-FRP beams compared to theoretical values of control beam B1. All beam specimens with FRP laminates increases the load carrying capacity of the beam. The addition of CFRP laminates was observed a lesser load value than other specimens because CFRP was more brittle compared to GFRP. Similarly B5 beam failed due to debonding of the FRP element.

3.3 Stiffness

The stiffness may be defined as the load required for unit deformation which can be calculated as the ratio between the load and its corresponding deformation. The stiffness degradation curve is shown in Fig. 7. B4 specimens enhanced the load carrying capacity and ductility irrespective of other specimens with no considerable improvement in stiffness. Such similar results were also obtained by (Hawileh *et al.* 2014b). Figure shows that stiffness is highly enhanced in B4 due to EB-FRP laminates.

3.4 Energy absorption capacity

The area under the load deflection curve represents the energy absorption capacity of the specimen. It plays a major role in failure pattern of members under static loading. From Fig. 8, the

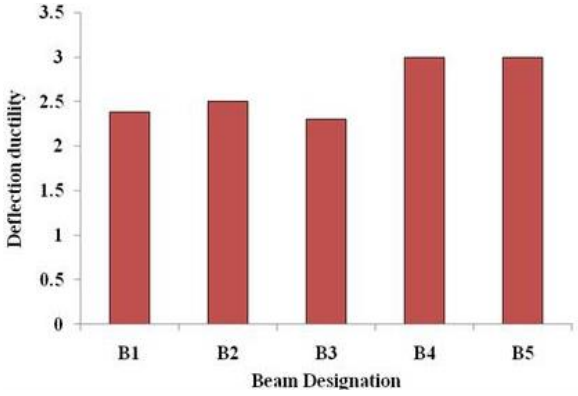

Fig. 9 Deflection ductility of the beams

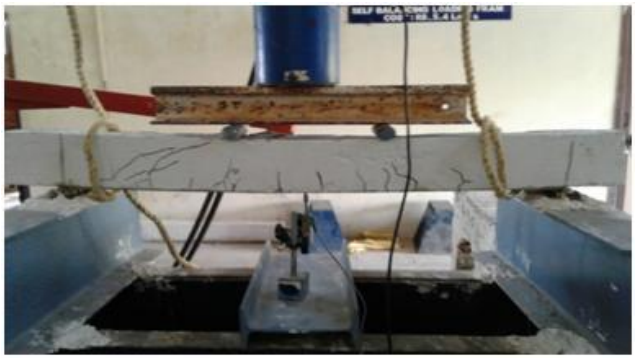

Fig. 10 Crack pattern of beams

total energy absorption capacity of B4 beam was more than 32.88% than control beam (B1) under flexural loading. Percentage increase in B3 is about 23.93% compared to B1. Similar improvement in B2 is about 37.92% compared to B1. Whereas in B4 the percentage increase is only about 18.16% compared to B1.

3.5 Deflection ductility

Ductility of a structure is its ability to undergo deformation beyond the initial yield deformation while still sustaining load. Ductility factor is the ratio between the ultimate deflection to the yield deflection. The displacement ductility factor of control and EB-FRP specimens are shown in Fig. 9. Beams (B2 and B3) strengthened with GFRP and CFRP specimen achieved a higher load capacity compared to the control specimen but failed at a lower mid-span deflection (less ductile). The beams strengthened with the composite EB-FRP (B4 and B5) achieved higher load carrying capacity and deflection than other specimen. The deflection ductility behaviors of beams in the present work are similar to the experimental work done by (Hawileh *et al.* 2014b). Among all the EB-FRP beams highest ultimate load and highest ductility was obtained for beam (B4). This shows that strengthening RC beams with composite EB-FRP would achieve a higher load carrying capacity and more ductile in nature. The deflection ductility of beams (B4 and B5) showed a maximum increase of about 26.1% when compared with the control beam (B1).

Table 4 Elements and their details

Material	Element	No of nodes
Concrete	SOLID 65	8
Steel	LINK 180	2
CFRP,GFRP	SOLID 185	8

Table 5 Property inputs for concrete and steel

Concrete	Properties
Young's modulus(kN/m^2)	2.23×10^4
Poisson's ratio	0.15
Open shear transfer co-efficient	0.23
Closed shear transfer co-efficient	0.9
Uniaxial cracking stress (kN/m^2)	2.5
Uniaxial crushing stress (kN/m^2)	-1
Steel bars	
Young's modulus of steel (kN/m^2)	2×10^5
Poisson's ratio	0.3
Yield stress	415

Table 6 Property input for GFRP and CFRP

Property		GFRP	CFRP
Elastic modulus(kN/m^2)	E_X	2.1×10^5	2.3×10^5
Poisson's ratio	PRXY	0.28	0.28
Shear modulus (kN/m^2)	G_{XY}	1520	11790

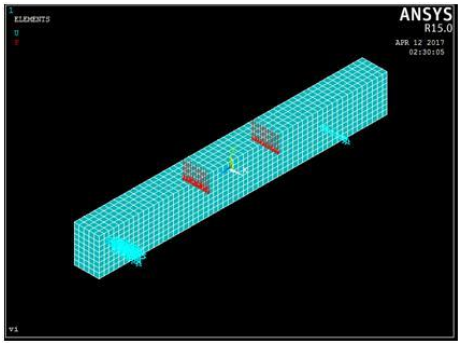

Fig. 11 Numerical model with boundary conditions

3.6 Modes of failure and crack pattern

Fig. 10 shows that the cracks at failure for EB-FRP are greater in numbers and more distributed over the span of the beam specimen. The control specimens failed in a flexure mode and crushing of concrete in the compression side in mid span of the beam. The beam specimen with EB-FRP

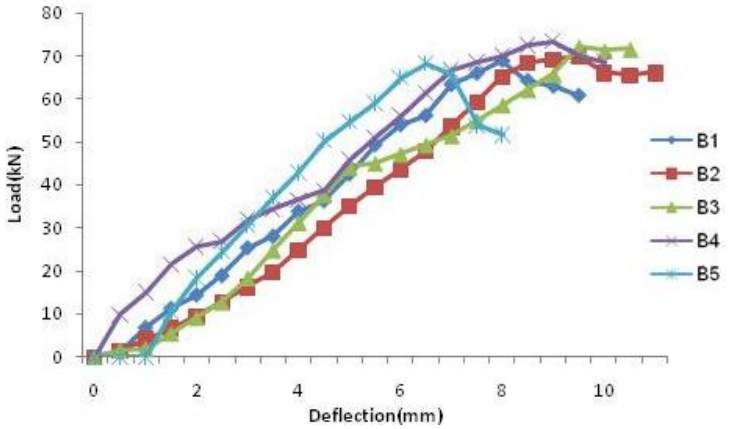

Fig. 12 Load deflection curves for the beams from numerical analysis

Table 7 Experimental and numerical deflection at ultimate load

Beam	Experimental Ultimate load (kN)	Numerical Ultimate Load (kN)	Prediction error [(Num/ Exp)-1]%	Experimental Deflection (mm)	Numerical Deflection (mm)	Prediction error [(Num/ Exp)-1]%
B1	65	66.93	2.96	9.5	9.44	-0.63
B2	70.12	69.9	-0.314	9.5	10.5	10.53
B3	68.02	71.1	4.52	10	10.76	7.6
B4	74.3	73.3	-1.34	10.5	10.12	-3.62
B5	64.1	68.1	6.24	7.5	7.55	0.67

failed by steel yielding followed by debonding. Such similar failure mode was also observed in the experimental study of (Hawileh *et al.* 2014b, Grace *et al.* 2002, Xiong *et al.* 2004). The visible flexural cracks developed at the ultimate load of each beam. All the beams exhibited a tension failure which is ductile failure including the control beam. As the beams are forced to deform further, the cracks became more pronounced and the concrete crushed one or both the ends and debonding also takes place. With further increase in beam deflection of the load decreased, accompanied by concrete spalling. This crack pattern is observed to be same for all the beams, except the number of cracks and the spacing of the cracks.

4. Numerical investigation

For the present work, the beams have a rectangular cross-section of 100 mm width, 150 mm height and 1200 mm length. The top longitudinal reinforcement consists of two hangar bars of 8mm diameter and the bottom longitudinal reinforcement consists of two bars of 12 mm diameter. The stirrups were made up of 6 mm bars at the spacing of 150 mm c/c. In ANSYS 15, the beams are created as elements as shown in Fig. 11. Symmetry of the beam was utilized for model. The elements involved in creating the model are Solid 65, Link 180 and Solid 185. The concrete beams were modeled as three dimensional elements Solid 65. Solid 185 were used for creating the model for the B2 and B3. Link 180 is a linear line element to be used as the element for the steel

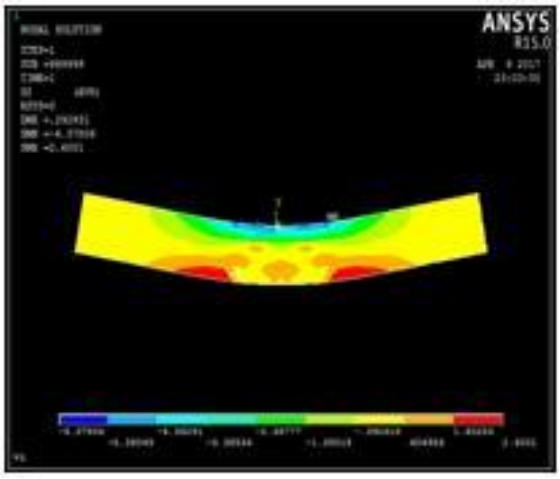

Fig. 13 Stress profile

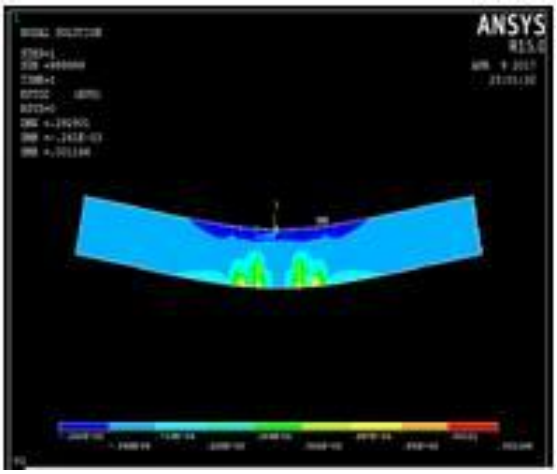

Fig. 14 Strain profile

reinforcements. In this element, shear deformation effects are included. The element details are given in Table 4. Property inputs for different materials are presented in Tables 5 and 6.

4.1 Load-deflection behavior of beams using ANSYS

Load deflection plot of the similar beams were carried out in ANSYS as shown in Fig. 12. Similar load deflection behavior was observed in numerical analysis, but the utilization of symmetry made the numerical model stiff compared to experimental beams. Percentage increase in ultimate load for B4 is 9.51% compared to B1. The ultimate load and deflection from model is shown in Table 7. The table clearly shows that for the beams strengthened with EB-FRP (B2, B3 and B4); load carrying capacity and deflection was increased compared to the control beam. Such similar results were also observed in the earlier study of (Hawileh *et al.* 2014b). For the beam (B5), the loading carrying capacity was increased substantially compared to the control beam (B1).

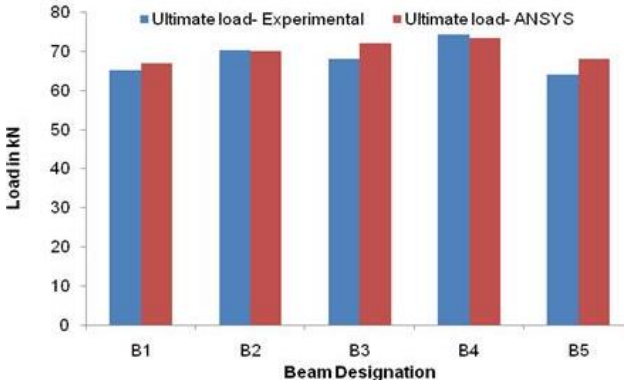

Fig. 15 Comparison of ultimate load between experimental and numerical analysis

However, the deformation was reduced as the failure occurred at the specimen. The comparison on the load carrying capacity up to ultimate load of experimental and numerical values were made. Fig. 12 inferred that ultimate load using numerical analysis more or less identical with the experimental results. Stress and strain distribution in beams is shown in Figs. 13 and 14, respectively. An EB-FRP beam reduces the shear stress in the concrete.

The load- deflection curve between experimental values and numerical analysis using ANSYS follows a similar qualitative curvature pattern for all the beams. Since the boundary conditions differ from experimental and numerical values. The values of ultimate load by numerical and experimental values had good correlation with the percentage error of about 10% respectively as shown in Fig. 15. The accuracy of numerical model to predict the load-deflection response was examined by comparing the predictions with the experimental results. Table 7 gives the ultimate load and ultimate deflection both experimentally and numerically. From Table 7, it is evident that there is a good correlation between experimental and numerical load-deflection curves at all stages of loading. The prediction error was calculated for ultimate load and deflection and the prediction error were within 6.24% and 10.53 % respectively. The numerical modeling was performed by (Hawileh *et al.* 2012d) on deep beams with externally bonded composites and the prediction error was calculated for load deflection responses till failure. The results were found to be more or less similar with the results of (Hawileh *et al.* 2012d).

5. Conclusions

Based on the experimental and numerical analysis the following conclusions are drawn

• From the results B4 beam and B2 beam has higher load carrying capacity in the experimental analysis and in the numerical analysis.

• The different failure modes were observed depending upon the type of FRP laminate used viz., concrete crushing, rupture and debonding of plates were observed.

• The ultimate load of the specimen with EB-FRP has increased in case of all the beams when compared to the control beam. However, comparing the trends observed in first crack load, the ultimate load, deflection ductility and the energy absorption capacity.

• The composite beam B4 and B5 shows enhanced ductility. The increase in deflection ductility was varied from 26.05% to 30.43%.

• Hence composite beam B4 is considered to have an optimum load carrying capacity, deflection ductility and energy absorption capacity both experimentally and numerically.

• Experimental test of control beams shows the wider cracks formed in the flexure region at bottom and crushing of concrete on top. In case of EB-FRP beams formation of cracks and increase of crack width is arrested at all load levels when compared with the control beam.

• During testing major flexural cracks appeared in the mid span of the beam and the failure was not catastrophic.

Acknowledgments

The authors acknowledge the Vice-Chancellor, SASTRA University for providing the facilities to carry out the work and the encouragement in completing this work. The authors are grateful to the anonymous reviewers for their valuable suggestions and comments that improved the quality of the present study.

References

Adil, A.T., Farid, H.A. and Abdulla, A.R. **(**2014), "Effects of harsh environmental exposures on the bond capacity between concrete and GFRP reinforcing bars", *Adv. Concrete Constr.*, **2**(1), 1-11.

Al-Rousan, R. and Haddad, R. (2013), "NLFEA sulfate- damage reinforced concrete beams strengthened with FRP", *Compos. Struct.*, **96**, 433-445.

Balsamo, A., Nardone, F., Iovinella, I., Ceroni, F. and Pecce, M. (2013), "Flexural strengthening of concrete beams with EB-FRP, SRP and SRCM: Experimental investigation", *Compos. Part B Eng.*, **46**, 91-101.

Barros, J.A.O. and Figueiras, J.A. (1996), *Flexure Behavior of SFRC: Testing and Modelling*, ISISE-Comunicações a Conferências Internacionais Magazine.

Chakrabortty and A. Khennane. (2014), "Failure mechanisms of hybrid FRP-concrete beams with external filament-wound wrapping", *Adv. Concrete Constr.*, **2**(1), 57-75.

Grace, N., Abdel-Sayed, G. and Ragheb, W. (2002), "Strengthening of concrete beams using innovative ductile fiber-reinforced polymer fabric", *ACI Struct. J.*, **99**, 692-700.

Hamid, R. and Allan, H. (2001), "Concrete beams strengthened with externally bonded FRP plates", *J. Compos. Constr.*, **5**, 44-56.

Hawileh, R.A., Hayder, A.R., Jamal, A.A. and Adil, K.A., (2014b) , "Behavior of reinforced concrete beams strengthened with externally bonded hybrid fiber reinforced polymer systems", *Mater. Des.*, **53**, 972-982.

Hawileh, R.A., Mohannad, Z.N. and Jamal, A.A. (2013c), "Finite element simulation of reinforced concrete beams externally strengthened with short-length CFRP plates", *Compos. Part B Eng.*, **45**, 1722-1730.

Hawileh, R.A., Obeidah, A.A., Jamal, A.A. and Adil, A.T. (2015a), "Temperature effect on the mechanical properties of carbon, glass and carbon-glass FRP laminates", *Constr. Build. Mater.*, **75**, 342-348.

Hawileh, R.A., Tamer, A.E.M. and Mohannad, Z.N. (2012d), "Nonlinear finite element modeling of concrete deep beams with openings strengthened with externally-bonded composites", *Mater. Des.*, **42**, 378-387.

Hong, K.N., Cho, C.G., Lee, S.H. and Park, Y.H. (2011), "Flexural behavior of RC members using externally bonded aluminum-glass fiber composite beams", *Polym.*, **6**(3), 667-685.

IS 2386 (1986), *Methods of Test for Aggregates for Concrete*, Bureau of Indian standards, New Delhi, India.

IS 383 (1970), *Specification of Coarse and Fine Aggregates from Natural Sources for Concrete*, Bureau of Indian Standards (BIS), New Delhi, India.

IS12269 (1997), *Specifications for 53 Grade Ordinary Portland Cement*, Bureau of Indian Standards, New Delhi, India.

Kolluru, V.S., Christian, C. and Lucio, N. (2007), "Width effect in the interface fracture during shear bonding of FRP sheets from concrete", *Eng. Fract. Mech*., **74**, 578-594.
Lesley, H.S., Salvatore, V., Christian, C. and Luciano, O. (2016), "Flexural behavior of RC beams strengthened with steel-FRCM composite", *Eng. Struct*., **127**, 686-699.
Prota, A., Tan, K.Y., Nanni, A., Pecce, M. and Manfredi, G. (2006), "Performance of shallow reinforced concrete beams with externally bonded steel-reinforced polymer", *ACI Struct. J*., 163-170.
Thomsen , H., Spacone, E., Limkatanyu, S. and Camata, G. (2004), "Failure mode analyses of reinforced concrete beams strengthened in flexure with externally bonded fiber-reinforced polymers", *J. Compos. Constr*., **8**, 123-132.
Xiong, G., Yang, J. and Ji, Z. (2004), "Behavior of reinforced concrete beams strengthened with externally bonded hybrid carbon fiber-glass fiber sheets", *J. Compos. Constr*., **8**, 275-278.

CC